arXiv:2004.01240v1 [cond-mat.mes-hall] 2 Apr 2020

Tunable Surface Plasmon Polaritons in a Weyl Semimetal Waveguide

S. Oskoui Abdol, A. Soltani Vala, B. Abdollahipour*
Department of condensed matter physics, Faculty of Physics, University of Tabriz, Tabriz 51666-16471, Iran
(Dated: November 17, 2021)

Weyl semimetals have recently attracted extensive attention due to their anomalous band structure manifested by topological properties that lead to some unusual and unique physical properties. We investigate novel features of surface plasmon polaritons in a slot waveguide comprised from two semi-infinite Weyl semimetals. We consider symmetric Voigt-Voigt and Faraday-Faraday configurations for plasmon polaritons in two interfaces of waveguide and show that the resulting dispersion is symmetric and the propagation of surface plasmon polaritons is bidirectional. We introduce exotic and novel asymmetric structures making use of difference in magnitude or orientation of chiral anomalies in two Weyl semimetals in both Voigt and Faraday configurations. These structures show a tremendous nonreciprocal dispersion and unidirectional propagation of surface plasmon polaritons. Moreover, we study an hybrid configuration of Voigt-Faraday for surface plasmon polartions in two interfaces of the waveguide. We find that this structure possesses unique futures. It shows surface plasmon polariton modes with unidirectional propagation above the bulk plasmon frequency. Furthermore, we find a surface plasmon polariton band which admits the Voigt and Faraday features simultaneously. Also, we show that the waveguide thickness and the chemical potential of the Weyl semimetals can be used as a fine-tuning parameters in these structures. Our findings may be employed in optical devices which exploit the unidirectional surface plasmon propagation features.

PACS numbers: 73.20.Mf, 78.68.+m, 42.79.Gn, 03.65.Vf

I. INTRODUCTION

The recent discovery of the topological insulators (TIs)[1,2] has led to a surge of interest in topological properties of the electronic band structure of crystalline materials. TIs exhibit a bulk gap, but gapless surface states protected by topology. Weyl semimetals (WSMs) being a non-trivial phase of matter have recently attracted extensive attention[3]. This interest is due to their anomalous band structure, which is manifested by topological properties[4] and protected Fermi arc surface states[5]. WSMs possess band structure touching at Weyl nodes, which appear in pairs and are characterized by linear dispersion close to the Fermi level[6]. In bulk Dirac semimetals (BDSs) Weyl nodes are doubly degenerate and are called Dirac nodes, which requires both time reversal and inversion symmetries to be conserved. In WSMs, breaking the time reversal symmetry or inversion symmetry leads to a separation of Weyl nodes with opposite chirality in momentum or energy, respectively. Weyl semimetal phase has recently been observed in TaAs[7], NbAs[8], NbP[9], $Eu_2Ir_2O_7$[10] and WTe_2[11]. Non-trivial band topology of WSMs emerges in a number of novel exotic effects such as chiral anomaly[12], anomalous Hall effect[13,14] and negative magnetoresistance[15]. Furthermore, chiral anomaly in WSMs is expected to result in the unusual optical responses due to the coupling of the electric and magnetic properties[16–20].

Surface plasmon polaritons (SPPs) are collective electromagnetic and electronic charge excitations which are confined to the interface of a metal or semiconductor with a dielectric[21]. SPPs propagate with wavelengths smaller than the light wavelength in vacuum and can be employed as a platform for developing novel plasmonic based optoelectronic devices such as surface plasmon resonance sensor[22] and scanning near field optical microscopy[23]. Application of an external magnetic field parallel to the interface of a metal or semiconductor with dielectric leads to a nonreciprocal SPP modes with a unidirectional propagating electromagnetic waves[24–27]. Also, unidirectional SPP mode has been reported in the system of two circularly polarized quantum emitters held above a metal surface[28]. The unidirectional electromagnetic wave propagation is the subject of chiral quantum optics which deals whit propagation-direction-dependent light-matter interactions[29]. Optical devices with the nonreciprocal SPPs are employed for developing unidirectional optical circuits[30] and the directed excitations in a ring laser[31].

Recently, SPP modes on the surface of a TI have been investigated theoretically[32–36] and experimentally[37,38]. SPP modes on TI surface exhibit the same dispersion relation as those of graphene due to their identical linear Dirac electronic spectra. On the other hand, the charge and spin density waves are coupled due to the spin-momentum locking in the TI, giving rise to spin-coupled surface plasmons or spin plasmons[32,33]. A ferromagnetic coupling or an external magnetic field brakes the time reversal symmetry of surface states in TI and causes a magneto-optical Kerr effect. This effect gives rise to generation of a novel transverse SPP in addition to the usual longitudinal one on the surface of a TI[34–36]. Several studies have been devoted to investigation of the surface plasmon polaritons in BDSs and WSMs. The properties of plasmon excitation in BDSs have been studied and it has been shown that these excitations are universal[39]. It has

*Corresponding author,
Email Address: b-abdollahi@tabrizu.ac.ir

been shown that in frequencies lower than the Fermi energy the metallic response is dominated in a BDS film and manifests in the existence of the SPPs, but at higher frequencies the dielectric response is dominated and it behaves as a dielectric waveguide[40]. SPPs behavior in the interface of a Bulk WSM and a dielectric has been studied for different orientations of the Weyl nodes separation vector and the SPP propagation direction[41]. It has been shown that the SPP dispersion depends on the Weyl nodes separation in energy or momentum space and for a time reversal broken WSM the Weyl nodes separation acts as an effective external magnetic field. Moreover, in the Voigt configuration SPP has a nonreciprocal unidirectional dispersion. In the Faraday and perpendicular configurations the SPP dispersion develops a gap at an intermediate frequency region. Further, studies have been performed for nonreciprocal propagation of SPP in Weyl semimetal thin films. The existence of giant nonreciprocal waveguide electromagnetic modes in WSM thin films in the Voigt configuration have been predicted[42]. Also, it has been shown that the SPP dispersion and its nonreciprocal property can be controlled by fine-tuning of the thickness of WSM thin film and dielectric contrast of the outer insulators[43]. Recently, the generation of SPPs at visible wavelengths in the WSM WTe_2 has been reported[44]. The nonreciprocal unidirectional propagation of the electromagnetic modes has been studied extensively in the context of magnetoplasmons in dielectric waveguides with ferrite substrate and films of magnetic dielectrics[45–47].

The inherent properties of the SPPs on the surface of WSM are caused by its intrinsic topological properties without need to application of high external magnetic fields (up to several tens of tesla). These topological properties fixes strength of the coupling of the electric and magnetic properties of WSMs through the chiral magnetic effect which depends on the separation of the Weyl nodes in momentum space. The transverse or Hall conductivity in these materials which is responsible for inhomogeneous optical responses of WSMs is estimated to be several orders of magnitude larger than typical magnetic dielectrics[42,43]. Therefore, the intrinsic topological properties of WSMs provide the opportunity to stable and efficient control of SPP propagation at the interface of these materials. Motivated by these intriguing properties of SPPs at the interface of a WSM, we intend to study SPP dispersion and localization in a WSM slot waveguide. Strong and intrinsic chiral magnetic effect in WSMs provides the opportunity to consider more achievable configurations in a WSM slot waveguide. We study symmetric Voigt-Voigt and Faraday-Faraday waveguides and show that as it is expected the SPP dispersion in these structures are reciprocal. Also, we find that a robust nonreciprocallity and unidirectional propagation of SPPs in Voigt-Voigt configuration can be achieved by contrasting the magnitude or direction of the chiral magnetic vectors in two WSMs. Further, we analyze the SPPs dispersion in the hybrid Voigt-Faraday configuration and again retrieve a giant nonreciprocal SPP propagation for frequencies above the bulk plasmon frequency. Moreover, we observe some novel and exotic features such as a SPP dispersion band which inherit simultaneously Voigt and Faraday configurations properties. Also, we show that the thickness of the slot waveguide and the chemical potential of the WSMs can be used as fine-tuning to control the SPPs propagation in these structures. These fascinating features being originated from intrinsic topological properties of the WSMs make them experimentally feasible and on the other hand may be very important from the practical perspective.

The remainder of the paper is organized as follows: In Sec. II we give some basic background about the optical responses of WSMs. Sec. III and its subsections have been devoted to present the derivation of dispersion relation for Voigt-Voigt, Faraday-Faraday and Voigt-Faraday configuration and discussing properties of SPP dispersion in these structures. Finally, we end by giving conclusion In Sec. IV.

II. THE THEORETICAL BACKGROUND

In the bulk of the WSM the valance and conduction bands touch each other at the Weyl nodes which appear in pairs with opposite chiralities. A WSM with broken time reversal symmetry contains two Weyl nodes with opposite chiralities separated in momentum space, while for a WSM with broken inversion symmetry Weyl nodes are separated in energy space. The low energy Hamiltonian in the vicinity of these points is given by[18],

$$\hat{H} = \chi v_F \sigma \cdot (\mathbf{k} - \mathbf{b}) + \chi b_0, \tag{2.1}$$

where v_F is the Fermi velocity, $\chi = \pm 1$ denotes the chirality, $\mathbf{k} = (k_x, k_y, k_z)$ is the momentum operator and $\sigma = (\sigma_x, \sigma_y, \sigma_z)$ is the vector of the Pauli matrices. $\mathbf{b}$ and b_0 indicate the separation of two Weyl nodes in momentum and energy, respectively. The topological properties of the WSM is explained by $\theta(\mathbf{r}, t) = 2(\mathbf{b}.\mathbf{r} - b_0 t)$ which is referred as *axion angle*[18]. For $\mathbf{b} = b_0 = 0$, the bands are degenerate and the material does not possess topological properties. It is the case of so called BDS. The axion angle effect is described by an additional term L_θ in the Lagrangian of the system[48],

$$\mathcal{L}_{em} = \frac{1}{8\pi}(\mathbf{E}^2 - \mathbf{B}^2) - \rho\varphi + \mathbf{J} \cdot \mathbf{A} + L_\theta, \tag{2.2}$$

$$L_\theta = -\frac{\alpha}{4\pi^2}\theta(r, t)\mathbf{E} \cdot \mathbf{B}, \tag{2.3}$$

where $\mathbf{E}$, $\mathbf{B}$, φ and $\mathbf{A}$ are the electric field, magnetic field, electric potential and magnetic vector potential, respectively. Here, the charge and current densities are denoted by ρ and $\mathbf{J}$. In the above equation α is a constant called effective fine structure constant of the WSM. Thus, the

resulting Maxwell's equations are,

$$\begin{aligned} \nabla \cdot \mathbf{E} &= 4\pi(\rho + \frac{\alpha}{2\pi^2}\mathbf{b}\cdot\mathbf{B}), \\ -\frac{1}{c}\frac{\partial \mathbf{E}}{\partial t} + \nabla \times \mathbf{B} &= \frac{4\pi}{c}[\mathbf{J} - \frac{\alpha}{2\pi^2}(c\mathbf{b}\times\mathbf{E} - b_0\mathbf{B})], \\ \nabla \times \mathbf{E} &= -\frac{1}{c}\frac{\partial \mathbf{B}}{\partial t}, \\ \nabla \cdot \mathbf{B} &= 0. \end{aligned} \tag{2.4}$$

As a result, the charge and current densities are modified in the Maxwell's equations by additional terms proportional to $-\nabla\theta\cdot\mathbf{B}$ and $\nabla\theta\times\mathbf{E}+\dot{\theta}\mathbf{B}$, respectively. So the displacement electric field is given by[41],

$$\mathbf{D} = (\varepsilon_\infty + \frac{4\pi i}{\omega}\sigma)\mathbf{E} + \frac{ie^2}{\pi\hbar\omega}(\nabla\theta)\times\mathbf{E} + \frac{ie^2}{\pi\hbar c\omega}\dot{\theta}\mathbf{B}\ , \tag{2.5}$$

where ε_∞ is the static dielectric constant of WSM and σ is the conductivity. First term of the above equation represents the displacement field for a normal metals, while the two last terms originate from chiral anomaly representing the anomalous Hall effect (AHE) and chiral magnetic effect (CME), respectively[3].

For a WSM with broken time reversal symmetry, the chiral anomaly causes an anisotropic optical response with the diagonal and off diagonal terms given by $\varepsilon(\omega) = \varepsilon_\infty(1 - \frac{{\Omega_p}^2}{\omega^2})$ and $\varepsilon_b(\omega) = \varepsilon_\infty\frac{\omega_b}{\omega}$, respectively. Where ${\Omega_p}^2 = \frac{4\alpha}{3\pi}(\frac{\mu}{\hbar})^2$ refers to bulk plasmon frequency with $\alpha = \frac{e^2}{\hbar v_f \varepsilon_\infty}$, μ chemical potential and $\omega_b = 2e^2\left|b\right|/\pi\hbar\varepsilon_\infty$. Measurements have been revealed an ultrahigh mobilities (much higher than the best graphene) and very small carrier scattering rates for BDSs and WSMs[9,10]. This mainly is due to the crystalline symmetries of these materials and their linear electronic dispersion relation around the Weyl nodes. Therefore, we have ignored the effect of the carrier scattering in the dielectric tensor of WSM and we disregard the effect of loss on SPP propagation in the subsequent calculations.

To study the SPP localized at the interface of a WSM and a dielectric, located at $x-y$ plane, we assume the electric field in the following form,

$$\mathbf{E} = (E_x, E_y, E_z)e^{iq_x x + iq_y y}e^{-i\omega t}e^{-\kappa|z|}. \tag{2.6}$$

This electric field decays exponentially away from interface in the z direction and propagates in the interface along the direction of $\mathbf{q} = (q_x, q_y)$. The decay constant $\kappa > 0$ is obtained by solving the wave equation,

$$\nabla\times(\nabla\times\mathbf{E}) = -\frac{1}{c^2}\frac{\partial^2}{\partial t^2}\mathbf{D}. \tag{2.7}$$

Substituting the electric field given by Eq.(2.6) in the wave equation (2.7) leads to a system of three linear equations,

$$\hat{M}\cdot\mathbf{E} = 0\ , \tag{2.8}$$

$$\hat{M} = \begin{pmatrix} q_y^2 - \kappa_j^2 & -q_x q_y & \mp i q_x\kappa_j \\ -q_x q_y & q_x^2 - \kappa_j^2 & \mp i q_y\kappa_j \\ \mp i q_x\kappa_j & \mp i q_y\kappa_j & {q_x}^2 + {q_y}^2 \end{pmatrix} - \frac{\omega^2}{c^2}\hat{\varepsilon}(\omega),$$

with the positive sign for the dielectric side and the negative one for the WSM side, $\hat{\varepsilon}$ denotes the dielectric tensor and $j = 1, 2$ refers to the different regions. The zeroes of the determinant of coefficient matrix ($\hat{M}$) yield the decay constants. There are different solutions for decay constant on the WSM side depending on the relative direction of the vectors $\mathbf{q}$ and $\mathbf{b}$[41]. The dispersion relation is obtained by applying boundary conditions at the interface which are continuity of the tangential components of the electric and magnetic fields.

SPPs are categorized in three different configurations according to the relative orientation of the vectors $\mathbf{b}$ and $\mathbf{q}$ whit respect to the surface: (a) Voigt geometry: $\mathbf{b}$ parallel to the surface, but perpendicular to $\mathbf{q}$ (b) Faraday geometry: $\mathbf{b}$ parallel to the surface and $\mathbf{q}$ (c) Perpendicular geometry: $\mathbf{b}$ perpendicular to the surface and $\mathbf{q}$. Here we consider the Voigt and Faraday configurations and their composition.

III. SURFACE PLASMON POLARITONS IN A SLOT WAVEGUIDE

The schematic structure of the system studied in the present paper has been depicted in Fig.1. This structure is composed of two semi-infinite layers of the WSM and an insulator layer with dielectric constant ε_d and thickness a in the middle. Optical properties of WSM layers are determined by a dielectric tensor which is intrinsic property of them in contrast to the semiconductor magneto optic materials in which the anisotropic response originates from an external magnetic field. The system of coordinates has been chosen so that the interfaces of WSMs and the middle dielectric to lie in the x-y plane and the z axis to be perpendicular to the interfaces. The relative orientation of the vectors in Voigt and Faraday Configurations has been shown in Fig.1 (b) and (c) as well. In the following sections we consider different situations combining Voigt and Faraday configurations and demonstrate the properties of the SPPs supported by these structures.

A. Surface plasmon polaritons in Voigt-Voigt waveguide

In this section we consider WSMs to be in the Voigt configuration. We assume the SPP propagation is in the y direction $\mathbf{q} = (0, q_y, 0)$ and for both WSMs we take $\mathbf{b}$ to be parallel with x axis, $\mathbf{b} = (b, 0, 0)$. Thus the dielectric tensors of mediums I and III (see Fig. 1) are given by,

$$\hat{\varepsilon}_{V,i}(\omega) = \begin{pmatrix} \varepsilon_i & 0 & 0 \\ 0 & \varepsilon_i & i\varepsilon_{bi} \\ 0 & -i\varepsilon_{bi} & \varepsilon_i \end{pmatrix}\ , i \equiv 1, 3 \tag{3.1}$$

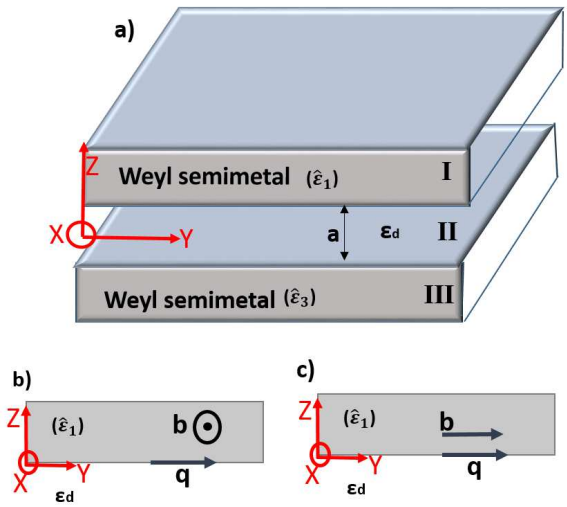


FIG. 1: (a) Schematic of a slot waveguide constructed of two semi-infinite WSMs connected by a dielectric layer with thickness a and dielectric constant ε_d. WSMs are considered in two different Voigt and Faraday configurations as illustrated in figures (b) the Voigt configuration and (c) the Faraday configuration.

Substituting the dielectric tensor in the wave equation, Eq. (2.7), we obtain the coefficient matrix $\hat{M}$ as,

$$\hat{M}_{V,i} = \begin{pmatrix} q^2 - {k_i}^2 - k_0^2\varepsilon_i & 0 & 0 \\ 0 & -{k_i}^2 - k_0^2\varepsilon_i & \mp iqk_i - ik_0^2\varepsilon_{bi} \\ 0 & \mp iqk_i + ik_0^2\varepsilon_{bi} & q^2 - k_0^2\varepsilon_i \end{pmatrix}. \tag{3.2}$$

Setting the determinant of $\hat{M}$ to zero, we obtain two solutions k_i^+ and k_i^- for decaying wave vector:

$$\begin{aligned} k_i^+ &= \sqrt{q^2 - k_0^2\varepsilon_i} \\ k_i^- &= \sqrt{q^2 - k_0^2\varepsilon_{vi}}\ , \end{aligned} \tag{3.3}$$

which are attributed to TE and TM modes, respectively. Where $\varepsilon_{vi} = (\varepsilon_i^2 - \varepsilon_{bi}^2)/\varepsilon_i$ is the Voigt dielectric constant and $k_0 = \omega/c$ is the vacuum wave vector. Since TE polarized waves are not affected by the chiral anomaly, similar to the magneto plasmons in the semiconductor magneto optic material[24], thus we consider only TM mode. A same procedure also gives the wave equation in the isotropic medium **II**, if we set diagonal elements of the dielectric tensor as $\varepsilon_{xx} = \varepsilon_{yy} = \varepsilon_{zz} = \varepsilon_d$ and off diagonal elements to zero. Therefore, the decay constant in the dielectric layer is obtained as $k_2 = \sqrt{q^2 - {k_0}^2\varepsilon_d}$. The electric field takes the following form throughout the structure,

$$\mathbf{E}(r,t) = \mathbf{E}(z)e^{i(qy-\omega t)} \tag{3.4}$$

The field amplitude in regions **I** ($z \geq a/2$), **II** ($-a/2 < z < a/2$) and **III** ($z \leq -a/2$) are expressed as follows:

$$\begin{cases} \mathbf{E}_1 = \begin{pmatrix} 0 & , E_{1y}e^{-k_1^-(z-a/2)} & , \beta_1 E_{1y}e^{-k_1^-(z-a/2)} \end{pmatrix} \\ \mathbf{E}_2 = \begin{pmatrix} 0 & , E_{2y}^+e^{+k_2 z} + E_{2y}^-e^{-k_2 z} & , \beta_2(E_{2y}^+e^{+k_2 z} - E_{2y}^-e^{-k_2 z}) \end{pmatrix} \\ \mathbf{E}_3 = \begin{pmatrix} 0 & , E_{3y}e^{+k_3^-(z-a/2)} & , \beta_3 E_{3y}e^{+k_3^-(z-a/2)} \end{pmatrix} \end{cases} \tag{3.5}$$

where $\beta_1 = \frac{E_{1z}}{E_{1y}} = -i\frac{(-qk_1^- + k_0^2\varepsilon_{b1})}{q^2 - k_0^2\varepsilon_1}$, $\beta_2 = \frac{E_{2z}}{E_{2y}} = -\frac{iqk_2}{q^2 - k_0^2\varepsilon_d}$ and $\beta_3 = \frac{E_{3z}}{E_{3y}} = -i\frac{(qk_3^- + k_0^2\varepsilon_{b3})}{q^2 - k_0^2\varepsilon_3}$. Imposing the continuity of tangential field components (E_y, H_x) as boundary conditions in two interfaces ($z = \pm a/2$) yields the following equations,

$$\begin{aligned} &e^{k_2 a/2}E_{2y}^+ + e^{-k_2 a/2}E_{2y}^- = E_{1y}, \\ &e^{k_2 a/2}E_{2y}^+ - e^{-k_2 a/2}E_{2y}^- = (-\tfrac{k_2\varepsilon_{w1}}{k_1^-\varepsilon_d})E_{1y}, \\ &e^{-k_2 a/2}E_{2y}^+ + e^{+k_2 a/2}E_{2y}^- = E_{3y}, \\ &e^{-k_2 a/2}E_{2y}^+ - e^{+k_2 a/2}E_{2y}^- = (-\tfrac{k_2\varepsilon_{w3}}{k_3^-\varepsilon_d})E_{3y}. \end{aligned} \tag{3.6}$$

Here $\varepsilon_{w1} = k_1^- \frac{-q\varepsilon_{b1} + k_1^-\varepsilon_1}{q^2 - k_0^2\varepsilon_1}$ and $\varepsilon_{w3} = k_3^- \frac{-q\varepsilon_{b3} - k_3^-\varepsilon_3}{q^2 - k_0^2\varepsilon_3}$. To obtain nonzero solutions for components of the electric fields E_{1y}, E_{2y}^+, E_{2y}^- and E_{3y}, determinant of the coefficient matrix of above equations should be zero. This leads to the dispersion relation of the Voigt-Voigt waveguide,

$$\frac{\varepsilon_d}{k_2}\left(-\frac{k_3^-}{\varepsilon_{w3}} + \frac{k_1^-}{\varepsilon_{w1}}\right) + \left[1 - \left(\frac{\varepsilon_d}{k_2}\right)^2\left(\frac{k_1^- k_3^-}{\varepsilon_{w1}\varepsilon_{w3}}\right)\right]\tanh(k_2 a) = 0. \tag{3.7}$$

Symmetric Voigt-Voigt waveguide: To study SPP in the symmetric waveguide, we set $\mu_1 = \mu_2 = \mu$ and $b_1 = b_2 = b$ which leads to the following quadratic dispersion equation in q:

$$\frac{\varepsilon_d}{k_2}\left(\frac{2\varepsilon k(q^2 - \varepsilon {k_0}^2)}{(\varepsilon k)^2 - (\varepsilon_b q)^2}\right) + \left[1 + (\frac{\varepsilon_d}{k_2})^2\frac{(q^2 - \varepsilon {k_0}^2)^2}{(\varepsilon k)^2 - (\varepsilon_b q)^2}\right]\tanh(k_2 a) = 0, \tag{3.8}$$

where we have defined $\varepsilon = \varepsilon_1 = \varepsilon_3$ and $\varepsilon_b = \varepsilon_{b1} = \varepsilon_{b3}$ and $k = k_1^- = k_3^-$. Therefore, the nonreciprocal effect reported in Ref[41] for the single interface of a WSM and a dielectric disappears in the symmetric waveguide structure due to the symmetry consideration and mixing of the SPPs at two interfaces.

In this case dispersion curves of the SPP have been plotted for different thicknesses $a = 0.1, 0.3, 0.5, 1, 3\ \mu m$ of the dielectric medium in Fig.2. In numerical calculation, we adopt a typical values for the parameters of WSMs as $\varepsilon_\infty = 13$, $\omega_b/\Omega_p = 0.5$, $E_f = 0.15\ eV$, $v_f = 10^6\ m/s$, $\Omega_p = 6.0918 \times 10^{13} s^{-1}$, measured for $Eu_2Ir_2O_7$[10,41] and $\varepsilon_d = 1$. As it can be seen from the figure, the dispersion curves of the SPP are composed of two bands which can be attributed to two distinct ways of the electron oscillations[49]. One of the bands appears below the bulk plasmon frequency and the other one above it, which hereafter we call them the lower and higher bands, respectively. The lower band starts from the origin and deviates from the light line of the dielectric layer

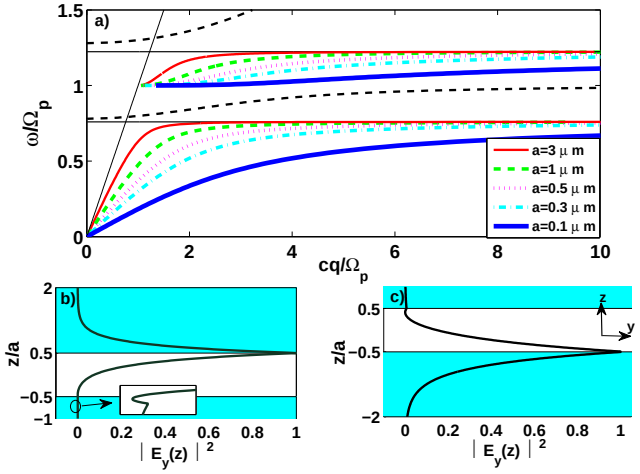


FIG. 2: a) Surface plasmon polariton dispersion of the symmetric slot waveguide in Voigt configuration with $\omega_b = 0.5\,\Omega_p$, $\varepsilon_\infty = 13$, $E_f = 0.15\ eV$, $v_f = 10^6\ m/s$, $\Omega_p = 6.0918\times10^{13}\,s^{-1}$ and $\varepsilon_d = 1$. In this plot, the bulk plasmon dispersion is indicated by black dashed line. The horizontal black solid thin lines indicate the asymptotic frequencies. The normalized electric field intensities of the SPP for thickness of $3\mu m$ and at frequencies 74.137 THz and 45.768 THz for b) the higher band and c) the lower band.

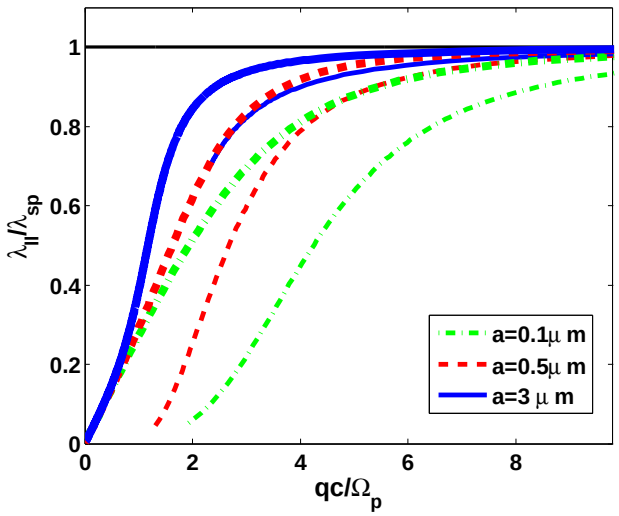


FIG. 3: The normalized localization length vs SPP wave vector of the symmetric slot waveguide in Voigt configuration with $\omega_b = 0.5\ \Omega_p$. Here λ_{ll} for lower and higher SPP bands are indicated by thick and thin lines, respectively.

and then it approaches to the asymptotic frequency in the large wave vectors. The higher band starts from the light line at $\omega = \Omega_p$ and immediately tends to its asymptotic frequency. As it has been shown in Fig. 2(a), by decreasing the thickness of the dielectric layer both SPP bands shift to the lower frequencies. In order to show the profile of the fields, we have displayed in Figs. 2(b) and 2(c) the normalized y component of the electric field intensity for lower and higher bands of SPP at frequencies 45.768 THz and 74.137 THz for the thickness 3 μm, respectively. It is obvious that the lower band of SPP has been highly localized at the lower interface ($z = -a/2$), while the higher band of SPP has been confined mostly to the upper interface ($z = +a/2$).

In the non-retarded limit ($|q| \gg k_0$), where $k = k_2 = q$, the dispersion relation is reduced to,

$$2\varepsilon_d\varepsilon + (\varepsilon_d^2 + \varepsilon^2 - \varepsilon_b^2)\tanh(|q|a) = 0. \qquad (3.9)$$

The asymptotic values of the dispersion curves denoted by thin black lines in Fig. 2(a) are solutions of Eq. (3.9) for $|q| \to \infty$,

$$\omega_{as}^{v} = \frac{\sqrt{\varepsilon_\infty^2\omega_b^2 + 4\varepsilon_\infty\Omega_p^2(\varepsilon_d + \varepsilon_\infty)} \pm \varepsilon_\infty\omega_b}{2(\varepsilon_d + \varepsilon_\infty)}, \qquad (3.10)$$

where positive (negative) sign is associated for higher (lower) bands. As it is obvious, for $\omega_b = 0$ the asymptotic frequencies of two bands are identical and they merge to one band, which means the WSM converts to a BDS. The normalized localization length ($\lambda_{ll}/\lambda_{sp} = q/k$), which characterizes decay of the electric field component of SPP away from the interface is plotted as a function of wave vector for different thicknesses of the dielectric layer in Fig. 3, where thick and thin lines correspond to the normalized localization length for lower and higher bands, respectively. As we expect, in this configuration the numerical results reveal that the decay constants are real quantity for all frequencies. As this figure shows, the localization length for both bands decreases by decreasing the thickness of the waveguide for intermediate wave vectors. For large wave vectors $qc/\Omega_p \gg 1$, localization length in all cases approaches to asymptotic value $\lambda_{sp} = 2\pi/q$.

Asymmetric Voigt-Voigt waveguide: Let us to consider an asymmetric waveguide constructed by two WSMs in the Voigt configuration having different **b** vectors, $\mathbf{b}_1 \neq \mathbf{b}_3$. We study two distinct cases of the difference in magnitude and orientation of the **b** vectors. First, we consider the case of contrast in the magnitude of the chiral anomalies $b_1 \neq b_2$. Thus, two WSMs have similar $\hat{M}$ matrix with $\omega_{b1} \neq \omega_{b3}$. Numerical solution of Eq.(3.7) gives dispersion curves for different thicknesses of the waveguide $a = 0.1, 0.3, 0.5, 3\ \mu m$ depicted in Fig. 4(a), (b), (c) and (d) for both $q > 0$ and $q < 0$. As we expect for an asymmetric waveguide the SPP dispersion is nonreciprocal, namely it depends on the propagation direction, due to the difference in magnitude of the chiral anomaly in WSMs. Our results show a tremendous range of frequency ($\Delta\omega \sim \Omega_p$) for unidirectional propagation of SPPs. This means that in a large range of frequency, which can be tuned through the chemical potential, SPP is propagated in one direction, while propagation of the SPP in the backward direction is forbidden. This property can be broadly used in realizing unidirectional optical circuits without need to use an external magnetic

field. As we can see from Fig. 4(a), (b), (c) and (d), by decreasing the thickness of the waveguide a global shift of the bands toward the lower frequencies is observed. For $q > 0$, the lower band starts from the origin and continuously approaches to the asymptotic frequency, but the higher band starts from the $\omega = \Omega_p$ and then tends to its asymptotic value. For $q < 0$, the starting points of the bands are similar to $q > 0$, but depending on the value of a the SPP bands may coincide with the bulk plasmon dispersion, which leads to developing a gap in the SPP dispersion. The gap of the dispersion in backward direction decreases by decreasing the thickness of the waveguide and for very small thicknesses gaps are closed completely. There is no SPP propagation in the frequencies inside the gap region, but it dose not restrict SPPs unidirectional propagation regarding the tunability of the gaps by the waveguide thickness.

To emphasis the tremendous range of frequencies of the unidirectional SPP propagation we obtain the asymptotic frequencies. In the nonretarded limit ($|q| \gg k_0$), we obtain the asymptotic frequencies for higher band,

$$\omega_{as}^{v+} = \frac{\sqrt{\varepsilon_\infty^2\omega_{b1}^2 + 4\varepsilon_\infty\Omega_p^2(\varepsilon_d+\varepsilon_\infty)} + \varepsilon_\infty\omega_{b1}}{2(\varepsilon_d+\varepsilon_\infty)} \quad for\ q>0, \tag{3.11}$$

$$\omega_{as}^{v-} = \frac{\sqrt{\varepsilon_\infty^2\omega_{b3}^2 + 4\varepsilon_\infty\Omega_p^2(\varepsilon_d+\varepsilon_\infty)} + \varepsilon_\infty\omega_{b3}}{2(\varepsilon_d+\varepsilon_\infty)} \quad for\ q<0, \tag{3.12}$$

and for the lower band,

$$\omega_{as}^{v+} = \frac{\sqrt{\varepsilon_\infty^2\omega_{b3}^2 + 4\varepsilon_\infty\Omega_p^2(\varepsilon_d+\varepsilon_\infty)} - \varepsilon_\infty\omega_{b3}}{2(\varepsilon_d+\varepsilon_\infty)} \quad for\ q>0, \tag{3.13}$$

$$\omega_{as}^{v-} = \frac{\sqrt{\varepsilon_\infty^2\omega_{b1}^2 + 4\varepsilon_\infty\Omega_p^2(\varepsilon_d+\varepsilon_\infty)} - \varepsilon_\infty\omega_{b1}}{2(\varepsilon_d+\varepsilon_\infty)} \quad for\ q<0. \tag{3.14}$$

These asymptotic frequencies have shown by thin black lines in Figs. (4). Considering the nonretarded limit of the SPPs dispersion it can be shown that the unidirectional propagation range grows monotonically by increasing contrast of two WSMs chiral anomalies. We illustrate aforementioned point by plotting $\Delta\omega = \omega_+ - \omega_-$ as a function of $|\omega_{b3} - \omega_{b1}|$ for lower and higher bands. As we can see in Fig. (5), for higher band the unidirectional propagation range grows very faster than the lower band. As a striking result we observe that a quite huge enhancement of nonreciprocal effect is accessible by using two different WSM materials in the slot waveguide. It is worth to mention that the chemical potentials of WSMs and waveguide thickness can be used as fine-tuning to acquire a prominent and robust nonreciprocal effect in the proposed structure without implementation of an external magnetic field.

Now we turn to the second case, namely difference in the $\mathbf{b}$ vectors directions. To realize it, we consider vector of nodes separation in two WSMs points in opposite directions $\mathbf{b_1} = -\mathbf{b_2} = \mathbf{b}$. For this situation the main Eq. 3.7 reduces to the following one,

$$2\varepsilon_d k/\left(k_2\varepsilon_{w1}\right) + \left[1 + {\varepsilon_d}^2k^2/\left({\varepsilon_{w1}}^2{k_2}^2\right)\right]\tanh(k_2a) = 0, \tag{3.15}$$

Numerical solution of this equation yields the SPP dispersion shown in Fig. 6 as a function of wave vector for different thicknesses of the waveguide. Our results tend to the SPP dispersion for a single interface of WSM and dielectric in the Voigt configuration at the wide waveguide limit. In this limit, for $q > 0$ the lower band starts from the origin an end when it intersects by the bulk plasmon dispersion, but the higher band starts from the light line above the bulk plasmon frequency and then tends to the asymptotic value. For $q < 0$ the lower band starts from the origin and continuously approaches to its asymptotic frequency, while the higher band starts from the light line and continues until it coincides with the bulk plasmon dispersion. Obviously, the dispersion is nonreciprocal and there is a range of frequencies with a unidirectional SPP propagation. As we can see from Fig. 6, decreasing the thickness of the waveguide leads to splitting of the higher and lower bands for $q > 0$ and $q < 0$, respectively. These splittings are due to the mixing of the SPP modes localized at two WSM interfaces and these split branches form a two nearly flat bands very close to the asymptotic frequencies. These nearly flat bands may be employed in slow light technology[49]. Furthermore, for $q > 0$ decreasing to very small thicknesses of the waveguide leads to merging of the lower band with lower split branch of the higher band at $\omega = \Omega_p$.

In the nonretarded limit, $|q| \gg k_0$, SPP dispersion equation reduces to the following equation,

$$2\varepsilon_d/\left(\varepsilon_1 - \varepsilon_{b1}\right) + \left(1 + \varepsilon_d^2/\left(\varepsilon_1 - \varepsilon_{b1}\right)^2\right)\tanh(|q|a) = 0. \tag{3.16}$$

The asymptotic frequencies are obtained by solving this equation in the limit of $|q| \to \infty$, which is identical with the result for a symmetric Voigt-Voigt configuration given by Eq. 3.10.

B. Surface plasmon polariton in a symmetric Faraday-Faraday waveguide

To study properties of the SPP dispersion in Faraday configuration, we consider a symmetric waveguide with two identical WSMs in Faraday configuration. In this case, direction of $\mathbf{b}$ is assumed to be parallel to the propagation direction $\mathbf{q}$ and both of them are taken to lie along y axis. Thus, dielectric tensors of WSMs in the Faraday configuration are given by,

$$\hat{\varepsilon}_F(\omega) = \begin{pmatrix} \varepsilon & 0 & i\varepsilon_b \\ 0 & \varepsilon & 0 \\ -i\varepsilon_b & 0 & \varepsilon \end{pmatrix}. \tag{3.17}$$

Substituting $\hat{\varepsilon}_F(\omega)$ in the wave equation results in a system of three linear equations resulting to a $\hat{M}$ matrix for

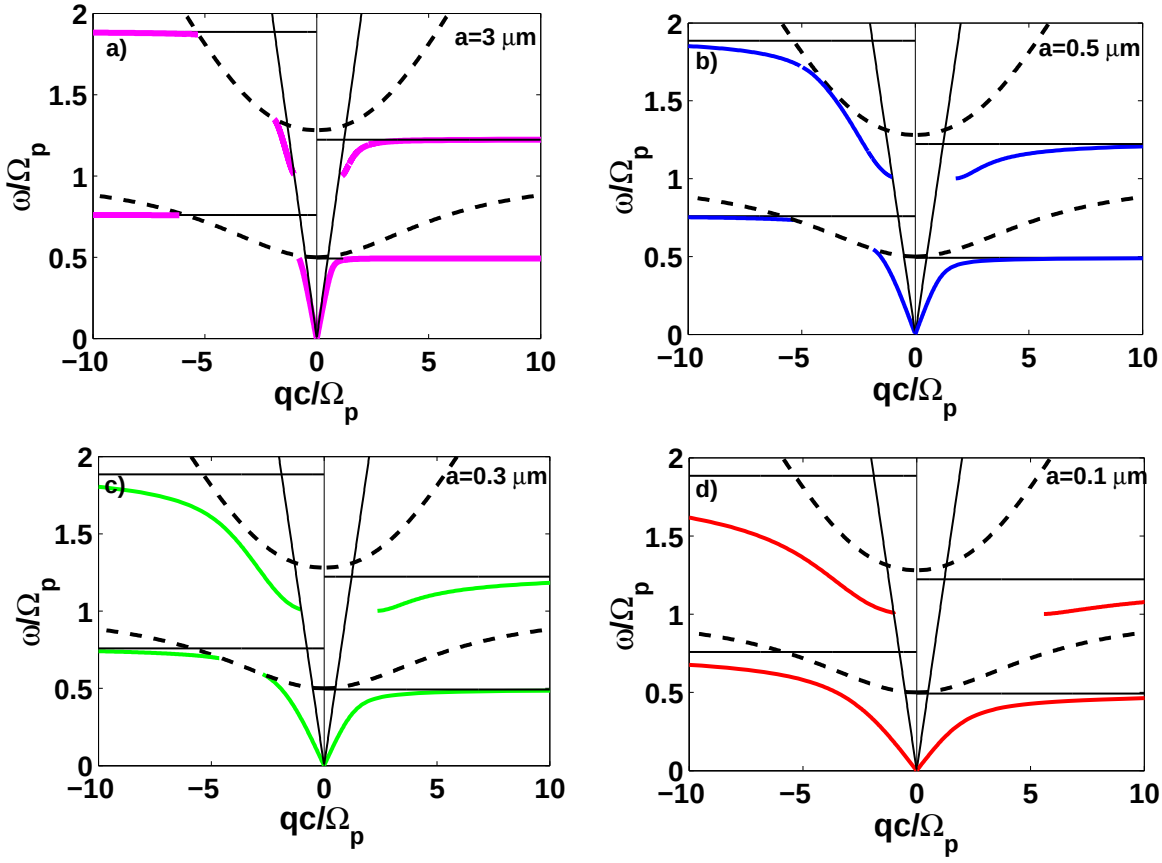


FIG. 4: SPP dispersion curve as a function of wave vector for the asymmetric Voigt-Voigt waveguide with $\omega_{b1} = 0.5\ \Omega_p$ and $\omega_{b3} = 1.5\ \Omega_p$ and the other parameter are similar to Fig.2. The black dashed lines show the bulk plasmon dispersion and the horizontal black solid thin lines indicate the asymptotic frequencies.

both mediums **I** and **III** as,

$$\hat{M}_F = \begin{pmatrix} q^2 - k^2 - \varepsilon k_0^2 & 0 & -ik_0^2\varepsilon_b \\ 0 & -k^2 - \varepsilon k_0^2 & \mp iqk \\ +ik_0^2\varepsilon_b & \mp iqk & q^2 - \varepsilon k_0^2 \end{pmatrix}. \quad (3.18)$$

Solutions for decaying wave vectors are obtained by making the determinant of $\hat{M}$ to be zero. As a result the decaying constants in both WSMs are given by,

$$k_\pm^2 = k^2 + k_0^2\left(\frac{\varepsilon_b^2}{2\varepsilon}\right) \pm \left[k_0^4\frac{\varepsilon_b^4}{2\varepsilon^2} + q^2k_0^2\frac{\varepsilon_b^2}{\varepsilon}\right]^{1/2}, \quad (3.19)$$

where $k^2 = q^2 - k_0^2\varepsilon$. So, components of the electric fields in three regions are expressed by,

$$\begin{cases} \mathbf{E}_1 = \left[E_{1x}^+ e^{-k_+(z-a/2)} + E_{1x}^- e^{-k_-(z-a/2)},\ \chi_+ E_{1x}^+ e^{-k_+(z-a/2)} + \chi_- E_{1x}^- e^{-k_-(z-a/2)},\ \eta_+ E_{1x}^+ e^{-k_+(z-a/2)} + \eta_- E_{1x}^- e^{-k_-(z-a/2)}\right], \\ \mathbf{E}_2 = \left[E_{2x}^+ e^{+k_2 z} + E_{2x}^- e^{-k_2 z},\ E_{2y}^+ e^{+k_2 z} + E_{2y}^- e^{-k_2 z},\ \beta(E_{2y}^+ e^{+k_2 z} - E_{2y}^- e^{-k_2 z})\right], \\ \mathbf{E}_3 = \left[E_{3x}^+ e^{k_+(z+a/2)} + E_{3x}^- e^{k_-(z+a/2)},\ \chi_+ E_{3x}^+ e^{k_+(z+a/2)} + \chi_- E_{3x}^- e^{k_-(z+a/2)},\ \eta_+ E_{3x}^+ e^{k_+(z+a/2)} + \eta_- E_{3x}^- e^{k_-(z+a/2)}\right], \end{cases} \quad (3.20)$$

where $\eta_\pm = \frac{E_{iz}}{E_{ix}} = \frac{q^2 - k_\pm^2 - k_0^2\varepsilon}{ik_0^2\varepsilon_b}$, $\chi_\pm = \mp A_\pm\left(\frac{qk_\pm}{k_0^2\varepsilon_b}\right)$, with $A_\pm = \frac{q^2 - k_\pm^2 - k_0^2\varepsilon}{k_\pm^2 + k_0^2\varepsilon}$. As the boundary condition, the tangential components of the electric and magnetic fields must to be matched at two interfaces. To do this we write the E_y, H_x and H_y components of fields in media I and III in terms of E_x in the same medium. Application of the boundary conditions results in the following

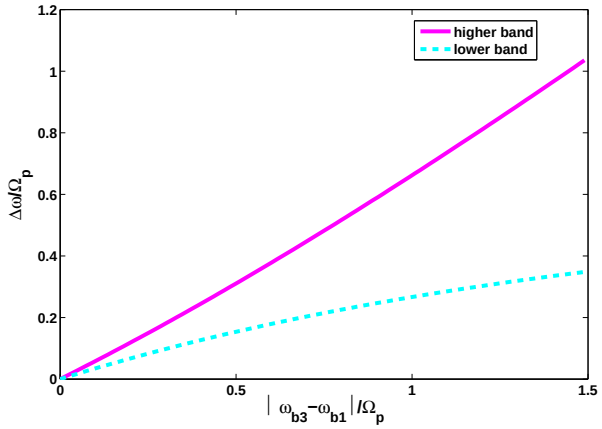


FIG. 5: Difference of the asymptotic frequencies of forward and backward propagation $\Delta\omega = \omega_+ - \omega_-$ as a function of $|\omega_{b3} - \omega_{b1}|$. Where we have considered $\omega_{b1}/\Omega_p = 0.5$ and the other parameters are similar to Fig. 2.

system of eight equations,

$$\begin{aligned}
&e^{k_2 a/2}E^+_{2x} + e^{-k_2 a/2}E^-_{2x} = E^+_{1x} + E^-_{1x},\\
&e^{k_2 a/2}E^+_{2y} + e^{-k_2 a/2}E_{2y-} = \left(\tfrac{-q}{k_0^2\varepsilon_b}\right)\left(A_+k_+E^+_{1x} + A_-k_-E^-_{1x}\right),\\
&e^{k_2 a/2}E^+_{2y} - e^{-k_2 a/2}E^-_{2y} = \left(\tfrac{qk_2\varepsilon}{k_0^2\varepsilon_b\varepsilon_d}\right)\left(A_+E^+_{1x} + A_-E^-_{1x}\right),\\
&e^{k_2 a/2}E^+_{2x} - e^{-k_2 a/2}E^-_{2x} = -\tfrac{k_+}{k_2}E^+_{1x} - \tfrac{k_-}{k_2}E^-_{1x},\\
&e^{-k_2 a/2}E^+_{2x} + e^{k_2 a/2}E^-_{2x} = E^+_{3x} + E^-_{3x},\\
&e^{-k_2 a/2}E^+_{2y} + e^{k_2 a/2}E^-_{2y} = \left(\tfrac{q}{k_0^2\varepsilon_b}\right)\left(A_+k_+E^+_{3x} + A_-k_-E^-_{3x}\right),\\
&e^{-k_2 a/2}E^+_{2y} - e^{k_2 a/2}E^-_{2y} = \left(\tfrac{qk_2\varepsilon}{k_0^2\varepsilon_b\varepsilon_d}\right)\left(A_+E^+_{3x} + A_-E^-_{3x}\right),\\
&e^{-k_2 a/2}E^+_{2x} - e^{k_2 a/2}E^-_{2x} = \tfrac{k_+}{k_2}E^+_{3x} + \tfrac{k_-}{k_2}E^-_{3x}.
\end{aligned} \tag{3.21}$$

Setting the determinant of its coefficient matrix to zero yields the dispersion relation as,

$$\begin{aligned}
&\big[\left(2\varepsilon_d\varepsilon {k_2}^2\left(2k_-k_+({A_-}^2+{A_+}^2) - A_-A_+(k_-+k_+)^2\right) + (-2A_-A_+\left({k_2}^2+k_-k_+\right)\left(\varepsilon^2{k_2}^2+\varepsilon_d^2k_-k_+\right)\right.\\
&\left.+{A_-}^2\left(\varepsilon^2{k_2}^2+\varepsilon_d^2{k_-}^2\right)\left({k_2}^2+k_+^2\right)+{A_+}^2\left(\varepsilon^2{k_2}^2+\varepsilon_d^2{k_+}^2\right)\left({k_2}^2+{k_-}^2\right))\tanh^2(k_2a)\right)\cosh^2(k_2a)\\
&+k_2(2A_-A_+\varepsilon_d\varepsilon k_2(k_--k_+)^2+(A_--A_+)\left(\varepsilon_d(A_-k_--A_+k_+)-\varepsilon(A_+k_-+A_-k_+)\right)\left(\varepsilon{k_2}^2+\varepsilon_dk_-k_+\right)\cosh(2k_2a))\big]=0\ .
\end{aligned} \tag{3.22}$$

It can be shown that in the nonretarded limit, Eq.(3.22) reduces to,

$$2\varepsilon_d\varepsilon + \left({\varepsilon_d}^2+\varepsilon^2\right)\tanh(qa) = 0, \tag{3.23}$$

and in this case, the asymptotic frequency reads, $\omega^F_{as} = \Omega_p\frac{\sqrt{\varepsilon_\infty}}{\sqrt{\varepsilon_d+\varepsilon_\infty}}$.

Dispersion curves of the symmetric Faraday- Faraday waveguide has been plotted in Fig.7 for different thicknesses of the dielectric $a = 3, 0.5, 0.3, 0.1\ \mu m$ as a function of SPP wave vector. As it can be seen from Fig.7, the SPP dispersion composes of two bands, one is very close to the SPP dispersion for a single interface with Faraday configuration, denoted by a red dotted curve, and the other one lies below it. For a wide waveguide these two bands merge into a one band coinciding with the result for a single interface. Decreasing the thickness of the waveguide leads to shifting of the lower band to the lower frequencies due to the mixing of the SPP modes of two interfaces. Further inspection reveals that the SSP modes are generalized surface waves, i.e. the decaying constants k_+ and k_- are complex conjugates of each other[24]. The Real and imaginary parts of the reduced decay constants $\beta_+ = k_+/q$ has been plotted as a function of the SPP wave vector for lower and higher bands of SPP dispersion in Figs. 8 (a), (b) and Figs. 8 (c), (d), respectively. As it can be seen, the real part of β_+ decreases with increasing of the wave vector and at large wave vectors it approaches to an asymptotic value for both bands. The imaginary part of the β_+ for both bands has a maximum in the intermediate wave vectors before approaching the asymptotic value at large wave vectors. The higher band has an interesting property that it has been composed of normal SPP modes (with vanishing imaginary part of the decaying constant) and generalized SPP modes.

C. Surface plasmon polariton in an asymmetric Voigt-Faraday waveguide

As an exotic structure, we consider an asymmetric waveguide comprising of two semi-infinite WSMs in two different Voigt and Faraday configurations. Since vector **b**, which plays a role similar to an external magnetic field in conventional semiconductor magneto optic materials, has different directions in two WSMs due to their different configurations, so the mentioned structure resembles to a waveguide placed in an external magnetic field having different directions in mediums I and III. Since chiral anomaly is an intrinsic property of the WSMs, the considered structure is experimentally achievable, while realizing such structure using external magnetic field may be a challenging task. This configuration exploits features of both Voigt and Faraday configuration simultaneously. It has been assumed that mediums I and III are in Voigt and Faraday configuration with dielectric tensors given by Eq. (3.1) and Eq. (3.17), respectively. The decay constant for the Voigt configuration (medium I) is given

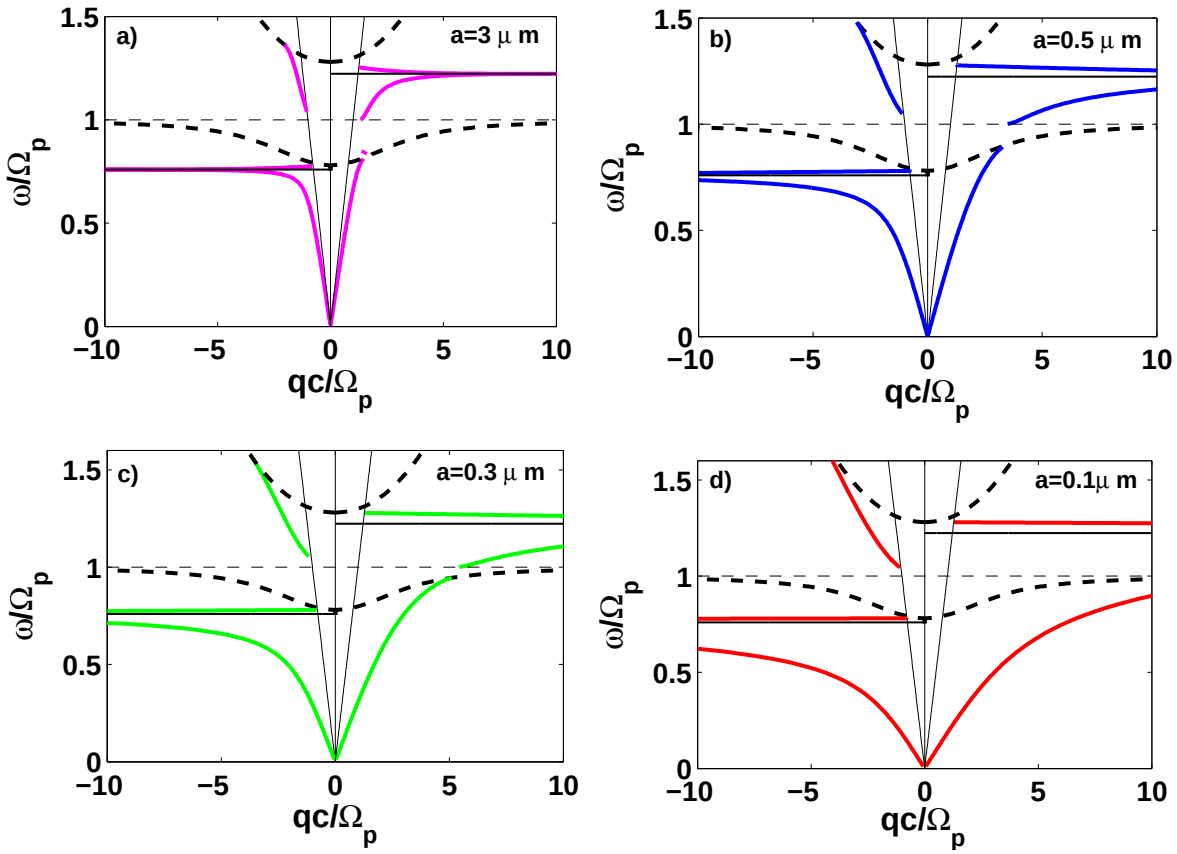


FIG. 6: SPP dispersion curve as a function of wave vector for the asymmetric Voigt-Voigt waveguide with antiparallel **b** vectors for $\omega_{b1} = \omega_{b3} = 0.5\ \Omega_p$ and the other parameters identical with Fig. 2. The black dashed lines show the bulk plasmon dispersion and the black solid thin lines indicate the asymptotic frequencies.

by Eq. (3.3) and for Faraday configuration (medium III) by Eq. (3.19). Therefore, components of the electric field in different mediums are expressed as,

$$\begin{cases} E_1(z) = \left[\ E_{1x}e^{-k_1^+}(z-a/2),\ \ E_{1y}e^{-k_1^-}(z-a/2),\ \ \beta_1 E_{1y}e^{-k_1^-}(z-a/2)\ \right], \\ E_2(z) = \left[\ E_{2x}^+e^{+k_2 z} + E_{2x}^-e^{-k_2 z},\ \ E_{2y}^+e^{+k_2 z} + E_{2y}^-e^{-k_2 z},\ \ \beta_2(E_{2y}^+e^{+k_2 z} - E_{2y}^-e^{-k_2 z})\ \right], \\ E_3(z) = \left[E_{3x}^+e^{k_3^+(z+a/2)} + E_{3x}^-e^{k_3^-}(z+a/2),\ \chi_+E_{3x}^+e^{k_3^+(z+a/2)} + \chi_-E_{3x}^-e^{k_3^-(z+a/2)},\ \eta_+E_{3x}^+e^{k_3^+(z+a/2)} + \eta_-E_{3x}^-e^{k_3^-(z+a/2)}\right], \end{cases} \tag{3.24}$$

where $\beta_1 = \frac{E_{1z}}{E_{1y}} = -\frac{(-iqk_1^- + k_0^2\varepsilon_b)}{q^2 - k_0^2\varepsilon}$, $\beta_2 = \frac{E_{2z}}{E_{2y}} = -\frac{iqk_2}{q^2 - k_0^2\varepsilon_d}$, $\eta_\pm = \frac{E_{3z}}{E_{3x}} = \frac{q^2 - k_3^{\pm 2} - k_0^2\varepsilon}{ik_0^2\varepsilon_b}$ and $\chi_\pm = \frac{E_{3y}}{E_{3x}} = A_\pm(\frac{+iqk_3^\pm}{ik_0^2\varepsilon_b})$ with $A_\pm = (\frac{q^2 - k_3^{\pm 2} - k_0^2\varepsilon}{k_3^{\pm 2} + k_0^2\varepsilon})$. Again by employing boundary conditions at two interfaces $z = \pm a/2$, eight linear equations are obtained for eight unknown amplitudes of electric filed $(E_{1x}, E_{1y}, E_{2x}^+, E_{2y}^+, E_{2x}^-, E_{2y}^-, E_{3y}^+, E_{3y}^-)$. Using the same procedure explained in the previous sections the following dispersion relation can be obtained for this structure,

$$\begin{aligned} &\left[-A_+\left(\varepsilon_d k_2\left(\varepsilon k_{1-} + \varepsilon_A k_{3+}\right) + \varepsilon\varepsilon_A k_d^2 T + \varepsilon_d^2 k_{1-}k_{3+}T\right)\left(k_2\left(k_{1+} + k_{3-}\right) + k_2^2 T + k_{1+}k_{3-}T\right)\right. \\ &\left.+A_-\left(\varepsilon_d k_2\left(\varepsilon k_{1-} + \varepsilon_A k_{3-}\right) + \varepsilon\varepsilon_A k_2^2 T + \varepsilon_d^2 k_{1-}k_{3-}T\right)\left(k_2\left(k_{1+} + k_{3+}\right) + k_2^2 T + k_{1+}k_{3+}T\right)\right]\cosh^2(k_2 a) = 0, \end{aligned} \tag{3.25}$$

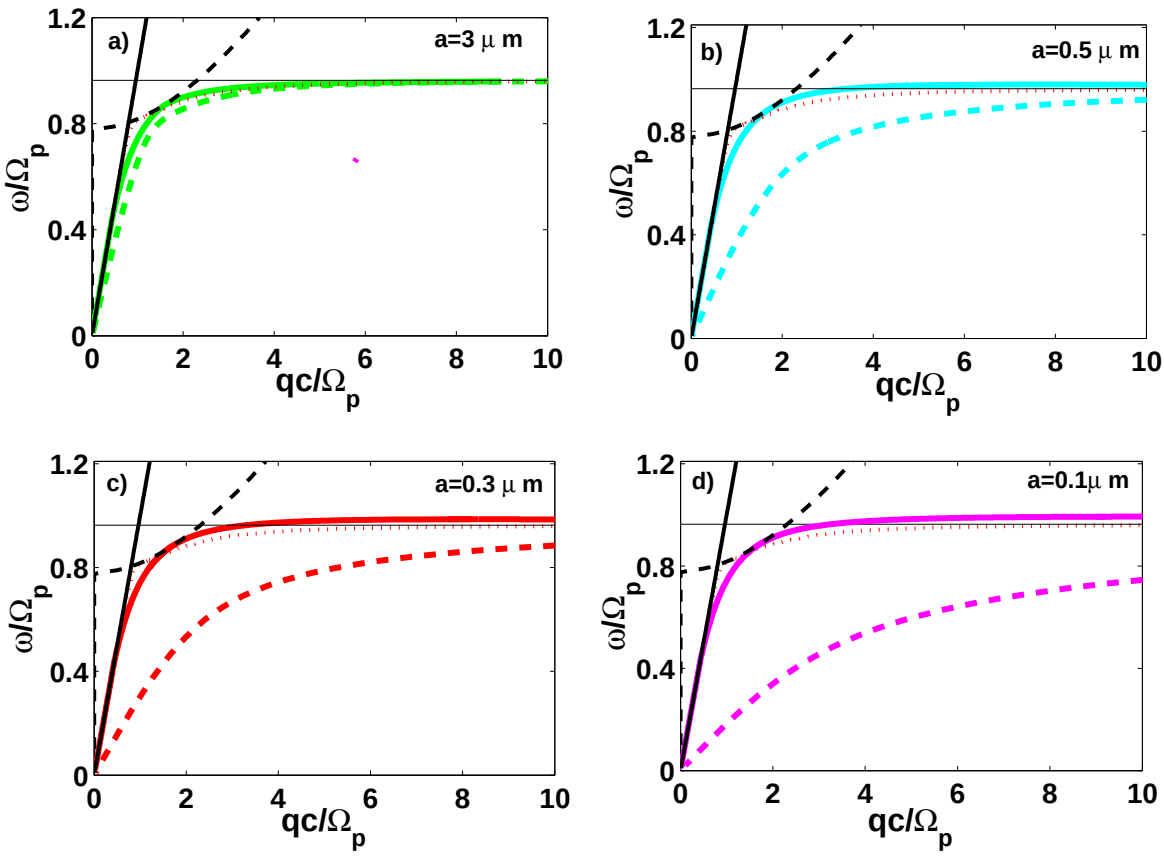


FIG. 7: The dispersion curves of the symmetric slot waveguide in the Faraday configuration with different thickness $a = 3, 0.5, 0.3$ and $0.1\ \mu m$. The other parameters are identical with Fig. 2.

where $T = tanh(k_2 a)$. In the nonretarded limit, Eq(3.25) reduces to,

$$\varepsilon_d\left(-2i\varepsilon+\varepsilon_b\right)+\left[\left(-i\varepsilon+\varepsilon_b\right)\varepsilon-i\varepsilon_d^2\right]\tanh(qa)=0. \tag{3.26}$$

For $aq \gg 1$, we end up with the following asymptotic frequencies,

$$\begin{aligned}\omega_{as}^{f} &= \Omega_p\frac{\sqrt{\varepsilon_\infty}}{\sqrt{\varepsilon_d+\varepsilon_\infty}}\\ \omega_{as}^{v} &= \frac{\Omega_p\omega_b\pm\sqrt{4\varepsilon_\infty\Omega_p^2(\varepsilon_\infty+\varepsilon_d)+\Omega_p^2\omega_b^2}}{2(\varepsilon_\infty+\varepsilon_d)}\end{aligned} \tag{3.27}$$

Fig. (9) shows the SPP dispersion for the asymmetric Voigt-Faraday waveguide for the dielectric thicknesses $a = 3, 1, 0.3, 0.1\ \mu m$. It is remarkable that the nonreciprocal effect - i.e., nonequivalent dispersion for positive and negative wave vectors - is observed in this configuration. As it is evident from Fig. (9), for a wide waveguide ($a = 3\mu m$) the dispersion curves are nearly identical with the results for a single interface between WSM and dielectric with Voigt and Faraday configurations[41]. The bands with Faraday character have two branches below the bulk plasmon frequency and are reciprocal, in contrast the bands possessing Voigt character are nonreciprocal with two higher and lower brands for forward propagation and a continues band for backward direction. In general the SPP modes above the plasmon frequency propagate unidirectional, while the SPP modes below the Ω_p are nonreciprocal but bidirectional. Decreasing the waveguide thickness leads to shifting the bands toward lower frequencies. An interesting result is merging the lower Voigt band with a branch of Faraday band close to Ω_p for $q > 0$ with decreasing the waveguide thickness, but the higher Voigt band retains its gap where it coincides with bulk plasmon dispersion. It leads to a continues band which posses the Voigt and Faraday characteristic simultaneously.

IV. CONCLUSION

In conclusion we have studied the SPP dispersion in a slot waveguide constructed by two WSMs connected via a dielectric layer. Here, we have considered novel and exotic configurations for SPP propagation due to the intrinsic topological properties of the WSMs. The symmetric Voigt-Voigt waveguide shows a reciprocal SPP dispersion. But, we showed that we can retrieve the non-

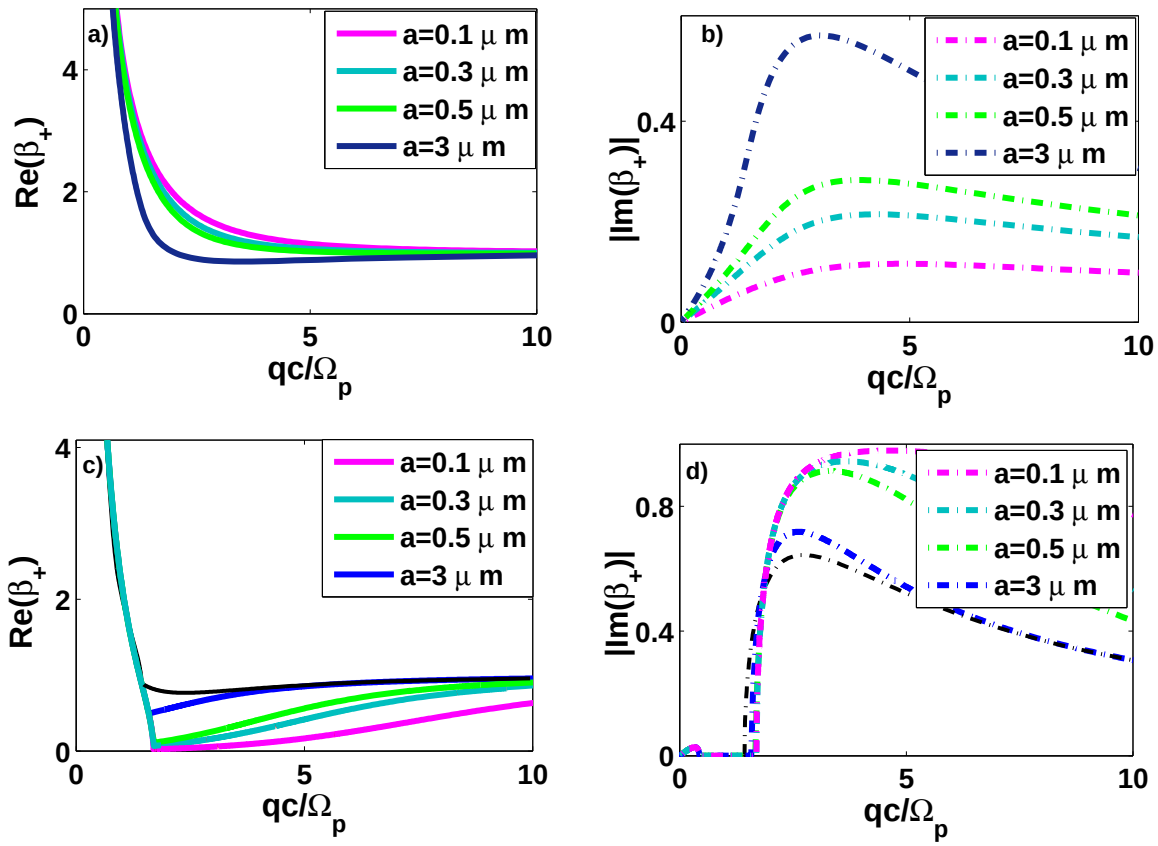


FIG. 8: a) Real and b) imaginary parts of the reduced decay constants Of lower band, c) real and b) imaginary parts of the reduced decay constants of higher band versus SPP wave vector in the symmetric slot waveguide with Faraday configuration for different thickness $a = 3, 0.5, 0.3$ and 0.1 μm.

reciprocal and unidirectional SPP propagation in Voigt configuration by breaking the symmetry of the structure via generating a contrast in chiral anomaly magnitude or its direction in two WSMs. It is remarkable that we observe a tremendous range of frequency for unidirectional SPP propagation. Furthermore, we showed that this unidirectional propagation can be fine-tuned by the waveguide thickness and the chemical potentials of two WSMs. Moreover, to complete our study we investigated the Faraday-Faraday waveguide which shows the reciprocal SPP dispersion with two bands below the bulk plasmon frequency. As an hybrid structure we studied the SPP dispersion in the Voigt-Faraday waveguide. We interestingly found that it shows a unidirectional SPP propagation above the bulk plasmon frequency, while it shows a nonreciprocal but bidirectional SPP dispersion below the bulk plasmon frequency. In summery, we observed a tremendous unidirectional SPP propagation in the structures introduced in this study. We believe that our results can be observed experimentally and they may be useful in creating unidirectional optical devices and in the slow light technology.

[1] Kane C L and Mele E J 2005 Phys. Rev. Lett. **95** 146802
[2] Hasan M Z and Kane C L 2010 Rev. Mod. Phys. **82** 3045
[3] Armitage N P, Mele E J and Vishwanath A 2018 Rev. Mod. Phys. **90** 015001
[4] Murakami S 2007 New J. Phys. **9** 356
[5] Wan X, Turner A M, Vishwanath A and Savrasov S Y 2011 Phys. Rev. B **83** 205101
[6] Fang Z, Nagaosa N, Takahashi K S, Asamitsu A, Mathieu R, Ogasawara T, Yamada H, Kawasaki M, Tokura Y and Terakura K 2003 Science **302** 92
[7] Xu S Y, Belopolski I, Alidoust N, Neupane M, Bian G, Zhang C, Sankar R, Chang G, Yuan Z, Lee C C, Huang S M, Zheng H, Ma J, Sanchez D S, Wang B, Bansil A, Chou F, Shibayev P P, Lin H, Jia S, and Hasan M Z 2015 Science **349**, 613
[8] Xu s Y, Alidoust N, Belopolski I, Yuan Z, Bian G, Chang T R, Zheng H, Strocov V N, Sanchez D S, Chang G, Zhang C, Mou D, Wu Y, Huang L, Lee C C, Huang S M, Wang

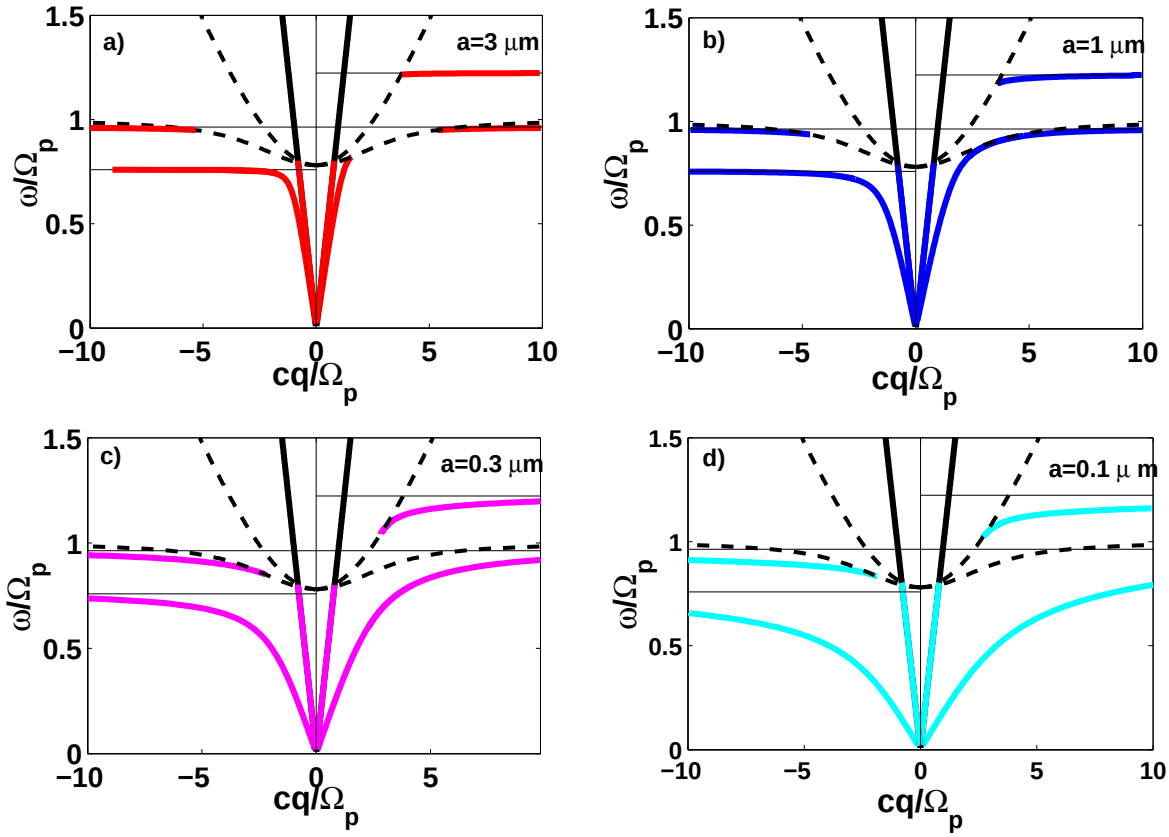


FIG. 9: Surface plasmon polariton of asymmetry Voigt-Faraday waveguide for different thickness of dielectric layer $a = 3, 1, 0.3$ and 0.1 μm. The other parameters are identical with Fig. 2.

B, Bansil A, Jeng H T, Neupert T, Kaminski A, Lin H, Jia S, and Zahid Hasan M 2015 Nat. Phys. **11**, 748

[9] Shekhar C, Nayak A K, Sun Y, Schmidt M, Nicklas M, Leermakers I, Zeitler U, Skourski Y, Wosnitza J, Liu Z, Chen Y, Schnelle W, Borrmann H, Grin Y, Felser C and Yan B 2015 Nat. Phys. **11**, 645-650

[10] Sushkov A B, Hofmann J B, Jenkins G S, Ishikawa J, Nakatsuji S, Das Sarma S, and Drew H D 2015 Phys. Rev. B **92**, 241108

[11] Wu Y, Mou D, Jo N H, Sun K, Huang L, Bud'ko S, P, Kaminski A 2016 Phys. Rev. B **94**, 121113(R)

[12] Parameswaran S A, Grover T, Abanin D A, Pesin D A and Vishwanath A 2014 Phys. Rev. X **4** 031035

[13] Xu G, Weng H M, Wang Z J, Dai X and Fang Z 2011 Phys. Rev. Lett. **107** 186806

[14] Burkov A A 2014 Phys. Rev. Lett. **113** 187202

[15] Huang X, Zhao L, Long L, Wang P, Chen D, Yang Z, Liang H, Xue M, Weng H, Fang Z, Dai X and Chen G 2015 Phys. Rev. X **5** 031023

[16] Zyuzin A A and Burkov A A 2012 Phys. Rev. B **86** 115133

[17] Chen Y, Wu Si and Burkov A A 2013 Phys. Rev. B **88** 125105

[18] Vazifeh M M and Franz M 2013 Phys. Rev. Lett. **111** 027201

[19] Ashby P E C, Carbotte J P 2013 Phys. Rev. B **87** 245131

[20] Ashby P E C and Carbotte J P 2014 Phys. Rev. B **89** 245121

[21] Maier S A, Plasmonics: Fundamentals and Applications (Springer, Berlin, 2007).

[22] Homola J, Yee S S and Gauglitz G 1999 Sens. Actuators B Chem. **54** 3

[23] Novotny L and Stranick S J 2006 Ann. Rev. Phys. Chem. **57** 303

[24] Wallis R F, Brion J J, Burstein E and Hartstein A 1974 Phys. Rev. B **9** 3424

[25] Kushwaha M S and Halevi P 1987 Phys. Rev. B **35** 3879

[26] Kushwaha M S and Halevi P 1987 Phys. Rev. B 36 5960

[27] Kushwaha M S 1987 Phys. Rev. B **36** 4807

[28] Downing C A, López Carreño J C, Laussy F P, del Valle E, and Fernández-Domínguez A I 2019 Phys. Rev. Lett. **122**, 057401

[29] Lodahl P, Mahmoodian S, Stobbe S, Rauschenbeutel A, Schneeweiss P, Volz J, Pichler H and Zoller P 2017 Nature **541**, 473-480

[30] Dötsch H, Bahlmann N, Zhuromskyy O, Hammer M, Wilkens L, Gerhardt R, Hertel P and Popkov A F 2005 J. Opt. Soc. Am. B **22** 240

[31] Kravtsov N V and Kravtsov N N 1999 Quantum Electron. **29** 378

[32] Raghu S, Chung S B, Qi X L, and Zhang S C 2010 Phys. Rev. Lett. **104**, 116401

[33] Efimkin D K, Lozovik Y E, and Sokolik A A 2012

Nanoscale Res. Lett. **7**, 163
[34] Karch A 2011 Phys. Rev. B **83**, 245432
[35] Schutky R, Ertler C, Trugler A, and Hohenester U 2013 Phys. Rev. B **88**, 195311
[36] Qi J, Liu H, and Xie X C 2014 Phys. Rev. B **89**, 155420
[37] Di Pietro P, Ortolani M, Limaj O, Di Gaspare A, Giliberti V, Giorgianni F, Brahlek M, Bansal N, Koirala N, Oh S, Calvani P, and Lupi S 2013 Nat. Nanotechnol. **8**, 556
[38] Lu H, Dai S, Yue Z, Fan Y, Cheng H, Di J, Mao D, Li E, Meia T and Zhao J 2019 Nanoscale **11**, 4759
[39] Kharzeev D E, Pisarski R D and Yee H U 2015 Phys. Rev. Lett. **115** 236402
[40] Kotov O V and Lozovik Yu E 2016 Phys. Rev. B **93** 235417
[41] Hofmann J and Das Sarma S 2016 Phys. Rev. B **93** 241402(R)
[42] Kotov O V and Lozovik Yu E, arXiv:1808.00342v1
[43] Tamaya T, Kato T, Konabe S and Kawabata S, arXiv:1811.08608v1
[44] Tan C, Yue Z, Dai Z, Bao Q, Wang X, Lu H and Wang L 2018 Opt. Mater. **86**, 421
[45] Chiu K W and Quinn J J 1972 Phys. Rev. B **5** 4707
[46] Hartstein A and Burstein E 1974 Solid State Commun. **14** 1223
[47] Kushwaha M S 2001 Surf. Sci. Rep. **41** 1
[48] Wilczek F 1987 Phys. Rev. Lett. **58** 1799
[49] Hu B, Wang Q J and Zhang Y 2012 Optic Express **20** 10072